Ferroelectric Hydration Shells around Proteins: Electrostatics of the Protein−Water Interface

David N. LeBard[†,‡] **and Dmitry V. Matyushov***[,†]

Center for Biological Physics, Arizona State University, PO Box 871604, Tempe, Arizona 85287-1604

Received: January 25, 2010; Revised Manuscript Received: May 3, 2010

Numerical simulations of hydrated proteins show that protein hydration shells are polarized into a ferroelectric layer with large values of the average dipole moment magnitude and the dipole moment variance. The emergence of the new polarized mesophase dramatically alters the statistics of electrostatic fluctuations at the protein−water interface. The linear response relation between the average electrostatic potential and its variance breaks down, with the breadth of the electrostatic fluctuations far exceeding the expectations of the linear response theories. The dynamics of these non-Gaussian electrostatic fluctuations are dominated by a slow (≃1 ns) component that freezes in at the temperature of the dynamical transition of proteins. The ferroelectric shell propagates 3−5 water diameters into the bulk.

1. Introduction

Despite several decades of intense research, the properties and principal relaxation modes of the protein−water interface remain a subject of intense interest and controversy. Several key phenomenological observations have been made, which gave initial insights into the nuclear modes and relaxation times involved in the interfacial dynamics and energetics. The combined results of Mössbauer and neutron scattering measurements have shown that rms displacements of the protein atoms change dramatically at the transition temperature $T_{tr} \simeq 200-240$ K[1−6] and to a lesser extent at a lower temperature, $T'_{tr} \simeq 150$ K.[7−9] The upper-temperature transition, labeled (somewhat broadly[4]) as the dynamical transition in proteins, marks an onset of anharmonic protein motions active at high temperatures, in contrast to purely phonon modes below T_{tr} (Figure 1a). In contrast, the low-temperature crossover at T'_{tr} appears when hydrogen bonds of the interfacial water start to break, allowing water rotations, also reflected by a change in the temperature slope of the heat capacity of partially hydrated proteins.[10] This is followed by the onset of water translations at about ≃160 K,[7] accompanied by a striking increase in the thermal expansion coefficient of the hydration layer.[11]

Which relaxation process/nuclear mode becomes active at high temperatures above T_{tr} is still debated.[5,8,12−15] The currently prevailing view[4,5,16] assigns the transition to the appearance, with increasing temperature, of a β-relaxation process[17] of the hydration shell in the observation window fixed by the instrument resolution. A nuclear mode producing this β-relaxation has not been clearly identified, but its collective nature, involving both the hydration shell and some surface motions of the protein, has been emphasized. Indeed, the transition temperature is the same for the protein and water components of the protein−water interface when their corresponding signals are recordered separately.[18,19] In addition, the collective relaxation process disappears when partially hydrated proteins are confined in a rigid matrix mostly affecting the hydration shells[20] or when the size of the polypeptide is reduced below some critical value.[21] It appears that this collective process does not require the presence of the protein tertiary and even secondary structure[21] and is probably generic to the interface between water and a flexible polymer with a chemically heterogeneous surface.[16,22] Even more generally, the observation of the dynamical transition in nonaqueous solvents (glycerol[23] and chloroform[24]) puts under question the necessity of the presence of water. The transition might be a general property of the interface between a mobile polar liquid and a more rigid polymer/colloid particle made of a less elastic material.

The dynamics of the protein−water and DNA−water interfaces were also probed by employing optical dyes linked to the biopolymer's surface.[26,29−32] The recordered property in this case is the Stokes shift dynamics, that is, the change in the position of the emission peak caused by the nuclear modes adjusting to a dipole moment created by dye's photoexcitation.[33] It was observed that, unlike for dyes dissolved in homogeneous polar solvents,[33] the Stokes shift dynamics of dyes at the water−biopolymer interface shows a slow ≃20−200 ps component (Figure 1b). It was suggested that this component is either a reflection of the same collective interfacial mode recordered by scattering experiments or a result of a slow water exchange between solvation shells.[30,34] Alternatively, the emergence of slow relaxation can be caused by waters pushed by protein conformational motions.[31,35,36] Indeed, when the observation window is broadened, one can observe increasingly slower relaxation components[32] reflecting a hierarchy of successively slower conformational motions of a biopolymer.

Given the importance of the protein−water interface to a number of protein functions, including folding and hydrophobic collapse,[37,38] the density profile of water at the protein surface has attracted much attention.[37,39,40] It was suggested that partial or complete dewetting of hydrophobic patches at the protein−water interface might be critical for folding.[41] Attraction interactions, existing also for hydrophobic residues, eliminate dewetting,[42−45] and the resulting density profile of interfacial water is an averaged reflection of the heterogeneous patchwork of hydrophobic and hydrophilic residues.[37,40] As a reflection of a partially broken network of hydrogen bonds, the compressibility of the protein solution is higher than that of bulk water[40] and also

* Corresponding author. E-mail: dmitrym@asu.edu.
† Arizona State University.
‡ Current address: Institute for Computational Molecular Science, Temple University.

10.1021/jp1006999
Published on Web 06/28/2010

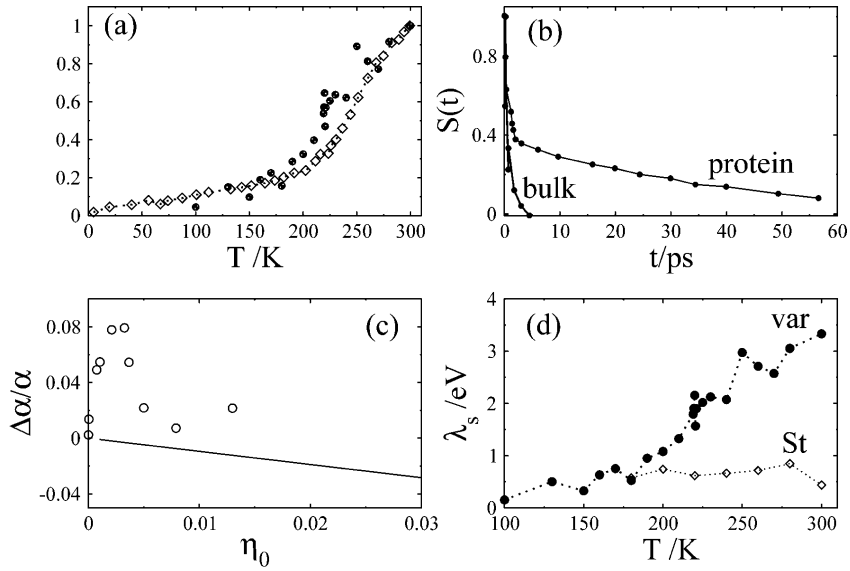

Figure 1. (a) Experimental msd displacement of the heme iron in myoglobin[2] (diamonds) and the solvent reorganization energy λ_s^{var} of plastocyanin from MD simulations[25] (circles) vs temperature. Both parameters are reduced to their corresponding values at 300 K. (b) The normalized Stokes shift correlation function of an optical dye in bulk water and at the protein−water interface (taken from ref 26). (c) The relative change in the terahertz dielectric absorption coefficient of the protein solution vs the volume fraction of the protein, η_0. The points are experimental data,[27] and the solid line is the prediction of dielectric theories neglecting the ferroelectric polarization of the water shell.[28] (d) Solvent reorganization energies λ_s^{var} (circles) and λ_s^{St} (diamonds) of plastocyanin from MD simulations.[25] The dotted lines in this plot connect the points.

correlates with a number of properties significant for protein stability, such as surface charge density and heat capacity of unfolding.[46,47]

Motivated by earlier Mössbauer and neutron scattering data reporting rms atomic displacements,[1−5] studies of protein dynamics have traditionally focused on the translational mobility of the interfacial water and the hydrogen bond dynamics,[48−50] both directly accessible from numerical computer simulations. This focus on interfacial density fluctuations is currently shifting toward studies of the interfacial electrostatics, a development driven by recent experimental advances in terahertz dielectric spectroscopy[21,27,51,52] and wider applications of conventional broad-band dielectric techniques.[5,16,20,53,54] Several important observations came from recent dielectric measurements.

First, a break in the temperature dependence of terahertz dielectric absorption,[52] reminiscent of the break in the rms atomic displacements, was obtained. This observation indicates that interfacial density and dipolar fluctuations share the same phenomenology. Second, an anomalous increase in the terahertz absorption coefficient was found for protein solutions at the protein volume fraction below 1% (Figure 1c).[27,55] This unexpected result was rationalized by assuming the electrostatic coherence between the protein and its hydration layers extending 15−20 Å into the bulk. An effective dipole moment of the protein and its hydration shell, much exceeding the dipole moment of the protein itself (see below), is required to explain these observations.[28]

Given these new experimental data and previous simulation reports of an unusual pattern of the dipolar polarization field around proteins,[56] one might expect some unconventional electrostatics of the protein−water interface. We indeed found[25] that the statistics of electrostatic potential fluctuations produced by hydration water inside proteins do not follow the commonly accurate[57,58] prescriptions of the linear response theory. According to the linear response, the average electrostatic potential of water taken at a probe charge q inside the protein can be connected to its variance by the fluctuation−dissipation relation, $\beta q\langle(\delta\phi)^2\rangle = -\langle\phi\rangle$.[58,59] This relation indeed holds for the electrostatic potential at the active site of the metalloprotein plastocyanin (PC) at low temperatures below T_{tr} but breaks down dramatically above T_{tr} (Figure 1d).[25] The variance deviates strongly upward from the average to the values normally not seen for small and rigid organic solutes. This paper aims to study the physical origin of this effect and to give a closer look at the statistics and dynamics of the dipolar polarization field at the protein−water interface. We show, in agreement with terahertz measurements,[27,55] that proteins are capable of polarizing nearest water shells and produce local ferroelectric order of water dipoles. This observation is a significant departure from the previous experience gathered in the field of solvation in molecular polar liquids. We start our discussion with a qualitative picture of how this finding affects observable properties linked to the interfacial electrostatics.

2. Picture of the Elastic Ferroelectric Shell

We have observed[25] fluctuations of the dipole moment of the protein's hydration shell far exceeding those in the bulk. This shell of an effectively higher polarity, which we have dubbed the "elastic ferroelectric shell", was suggested to produce the unusual statistics of the electrostatic potential at the interface and inside the protein. The term "ferroelectric" does not reflect the existence of a global symmetry breaking and a well-defined order parameter of conventional bulk ferroelectrics.[60] The dipole moment of the shell, $\mathbf{M}_s$, fluctuates in magnitude and rotates, resulting in $\langle\mathbf{M}_s\rangle = 0$ on the infinite observation time of the canonical ensemble, whereas $\langle M_s\rangle \neq 0$ due to the fluctuations of the dipole moment. If the observation time is shorter than the dynamics of $\mathbf{M}_s$, one observes a nonvanishing dipole moment $\langle\mathbf{M}_s\rangle_{obs} \neq 0$ on the observation time window indicated by the subscript. This phenomenology appears for any finite system, since the time of transition between different orientational phases (such as orientations of the ferroelectric director) becomes infinite only in the thermodynamic limit.[61] In other words, the ferroelectric director has a finite relaxation time for a ferroelectric domain. Such a water domain, elastically stressed

by motions of the protein, is what the elastic ferroelectric shell is describing.

We prefer the usage of the term "ferroelectric" in contrast to "polarized" (even though both terms are used interchangeably in the paper) because the polarization of the water cluster does not seem to be directly linked to the electric field of the protein and is, in fact, fairly insensitive to the overall protein charge and the surface charge density. Although a complete set of conditions responsible for the appearance of the ferroelectric shell is currently hard to track down, these are most likely related to the size, elasticity, and chemical heterogeneity of the protein surface. Whereas all of them can potentially contribute to the observables, one property of the protein electrostatics, the variance of the protein dipole moment, emerges from our analysis as a key parameter controlling the dipole moment fluctuations of the hydration shell.

Before going into a more detailed discussion, we briefly summarize the electrostatic parameters recordered from the simulation trajectories. Since we want to connect our observations to experimentally measurable properties of redox proteins, we consider an electrochemical half reaction in which the oxidation state of the copper metal in the active site of the plastocyanin redox protein is changed by depositing an electron from the oxidized (Ox) to reduced (Red) form. The deposition of an electron changes partial charges of a number of atoms in the protein's active site. These atoms can therefore be assigned difference charges Δq_j such that $\Sigma_j \Delta q_j = -1$.[66] These difference charges of the active site (denoted by "0") interact with the partial charges of the medium (denoted as "m") producing the Coulomb interaction energy V_{0m}. The medium is composed of the protein matrix ("p") and the hydration water (solvent, "s") such that the overall Coulomb energy is: $V_{0m} = V_{0p} + V_{0s}$.

The average interaction energy, $E_i = \langle V_{0m} \rangle_i$, can be calculated in each redox state enumerated as $i = 1$ and 2. Since Δq_j are the difference charges between two redox states, E_i are Coulomb components of the average optical (vertical) transition energies between the two redox states.[58,59,62−64] The difference of E_2 and E_1, known in spectroscopy as the Stokes shift, defines the Stokes shift reorganization energy $\lambda^{St} = (E_2 - E_1)/2$.[63] On the other hand, one can calculate the variance of the interaction potential V_{0m} in each state. This variance, according to the linear response approximation, is independent of the state used for the ensemble average, $\langle (\delta V_{0m})^2 \rangle_1 = \langle (\delta V_{0m})^2 \rangle_2$. Moreover, the static limit of the fluctuation−dissipation theorem[65] gives an alternative definition of the reorganization energy, labeled as λ^{var}, from the temperature-reduced variance[58,59]

$$\lambda^{var} = \beta \langle (\delta V_{0m})^2 \rangle / 2 \tag{1}$$

where $\beta = 1/(k_B T)$ is the inverse temperature.

The two definitions are, of course, identical within the linear response approximation and $\lambda^{var} = \lambda^{St}$. What was instead found from MD simulations of plastocyanin,[25,66] reaction center protein of bacterial photosynthesis,[67] and some other protein complexes[58,68] is that at $T > T_{tr}$ (Figure 1d)

$$\lambda^{var} \gg \lambda^{St} \tag{2}$$

Before presenting our quantitative findings below, we explain here this observation in terms of a qualitative picture of the ferroelectric elastic shell.

In the present paper, we report the statistics of electrostatic fluctuations due to both water and protein motions. Correspondingly, the Stokes shift reorganization energy is a sum of the water (s) and protein (p) components,

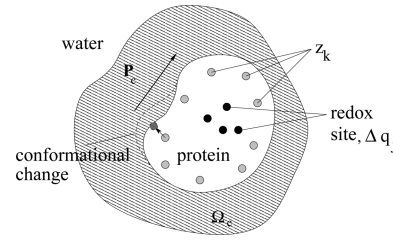

Figure 2. Cartoon of the polarized shell surrounding the protein. The ferroelectric shell with the volume Ω_c has a nonzero net polarization $\mathbf{P}_c$ producing the dipole moment $\mathbf{M}_c = \mathbf{P}_c \Omega_c$. The charges z_k belong to ionized surface residues not affected by changing redox state of the protein, whereas difference charges Δq_j of the active site reflect the change in partial atomic charges upon depositing the electron to the active site. These charges are used to calculate the Coulomb interaction potential V_{0s} with the surrounding water molecules and the interaction energy V_{0p} with the protein partial charges. The dashed line at the protein surface indicates a conformational motion shifting the corresponding surface charge and producing an elastic deformation of the ferroelectric cluster that propagates into a fluctuation of the polarization field $\mathbf{P}_c$.

$$\lambda^{St} = \lambda_s^{St} + \lambda_p^{St} \tag{3}$$

The variance reorganization energy contains, apart from the direct contributions from the water (λ_s^{var}) and protein (λ_p^{var}) fluctuations, the cross term λ_{sp}^{var} from cross-correlations between V_{0s} and V_{0p}

$$\lambda^{var} = \lambda_s^{var} + \lambda_p^{var} + \lambda_{sp}^{var} \tag{4}$$

Further, the Stokes shift reorganization energy of each component, protein and water, is related in the linear response approximation to the corresponding direct variance and the cross-correlation term

$$\lambda_{s,p}^{St} = \lambda_{s,p}^{var} + \frac{1}{2}\lambda_{sp}^{var} \tag{5}$$

We first focus on the question of how the change in the statistics of the water fluctuations affects the linear response relations listed here. To make our arguments more transparent, let us assume for the moment that dipolar polarization $\mathbf{P}_c$ is constant throughout the ferroelectric cluster with the average thickness L surrounding the protein (Figure 2). This shell polarization is an intrinsic property of the protein−water interface, which might be stabilized by ionized surface residues carrying charges z_k (Figure 2). Therefore, to a first approximation, $\mathbf{P}_c$ is not affected by the changing redox state of the active site

$$\mathbf{P}_{c,1} \simeq \mathbf{P}_{c,2} \tag{6}$$

This condition implies no contribution to the Stokes shift from cluster's polarization, since it will cancel out in the difference of average energies E_i. The entire Stokes shift will arise from slight reorientations of the water dipoles in response to the changing electric field of the active site. This linear polarization Stokes shift, typically considered in linear theories of molecular

redox reactions,[69] can be adequately calculated by standard models of polar solvent response, as we indeed found for hydrated plastocyanin.[64,66]

As we show below, the polarization field $\mathbf{P}_c$ is not static and changes both in magnitude and orientation. The relaxation of $\mathbf{P}_c$ might come from both the internal dynamics of water[70,71] and low-frequency vibrations of the protein elastically stressing the hydration shell.[72] The amplitudes of the protein vibrations increase sharply above T_{tr}, and so do the elastic motions of the hydration shell. The electrostatic effect of these collective motions, involving hundreds of water molecules ($\langle N^I \rangle \simeq 510$ waters in the first solvation layer of plastocyanin), develops into a gigantic[66] reorganization energy λ_s^{var}. Since, as we have stated above, these collective motions do not affect λ_s^{St}, the linear response equality between λ_s^{var} and λ_s^{St} breaks down, and one arrives at inequality 2.

One can estimate the result of fluctuations of the ferroelectric shell on the second-cumulant reorganization energy by averaging over the orientations of $\mathbf{P}_c$ in eq 1. This yields

$$\lambda_s^{var} = \lambda_s^{St} - (1/2)\lambda_{sp}^{var} + (\beta/6)(M_c\bar{E}_0)^2(2P_2 + 1) \quad (7)$$

The second term in this equation includes the total dipole moment $M_c = \langle P_c\Omega_c \rangle$ of the polarized cluster with the volume Ω_c and the electric field $\mathbf{E}_0(\mathbf{r})$ of the difference charges Δq_j averaged over the cluster's volume

$$\bar{\mathbf{E}}_0 = \Omega_c^{-1} \int_{\Omega_c} \mathbf{E}_0(\mathbf{r})\, d\mathbf{r} \quad (8)$$

The parameter P_2 is the second-order (nematic) order parameter of the polarization vector $\mathbf{P}_c$ defined relative to some chosen direction (the protein dipole moment, frozen on the time scale of water fluctuations, is used in the analysis below).

The notion of the constant polarization $\mathbf{P}_c$ is an oversimplification used here to outline the physical picture of the shell polarization. The emergence of a net water polarization is really an interfacial phenomenon, with the polarization $P_c(r)$ decaying approximately as $1/r^2$ with the distance r from the protein surface to the bulk. Most of the water polarization occurs in the first solvation layer, and this effect propagates into the adjacent water shells. The subensemble of $\langle N^I \rangle \simeq 510$ water molecules in the first solvation layer has a strong tendency to in-plane alignment of the dipoles[73] and to form 1D dipolar chains.[74,75] Whether the soft nuclear mode producing the net ferroelectric dipole can be traced back to a uniform polarization[76] or to an alignment of 1D dipolar chains,[74] there is a tendency to a ferroelectric transition of pseudospins describing water orientations in the surface layer.[74−77] Typically, expected signatures of such transitions (even though not in the thermodynamic limit) include critical slowing down of the principal nuclear mode and peaks in second cumulants of thermodynamic parameters.[78] We have, indeed, found[25] a critical slowing of the collective component of the Stokes shift dynamics and a sharp spike in λ_s^{var}, both singularities seen at T_{tr}. The nanometer size of proteins might be an important factor in creating the net dipolar interfacial polarization. On one hand, the size of a typical protein is sufficiently large to put several hundreds of waters in its first hydration layer. On the other hand, the finite size of this cluster eliminates long-wavelength phonons destroying the long-range order in infinite 2D systems.

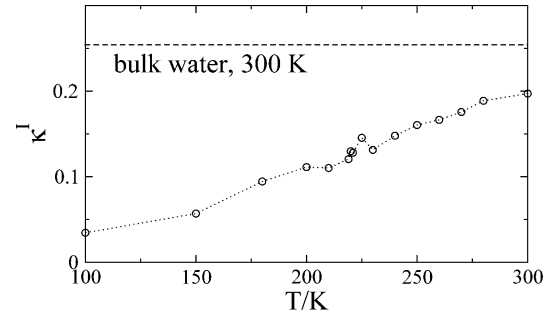

Figure 3. Normalized variance $\kappa^I = \langle(\delta N^I)^2\rangle/\langle N^I\rangle$ vs temperature for the number of water molecules N^I in the first solvation layer of plastocyanin. The dashed line shows the result for bulk TIP4P water at 300 K reported by Mittal and Hummer.[43] A somewhat smaller value of 0.2 was reported by Sarupria and Garde[45] for SPC/E water. We note that from an approximately linear trend of κ^I with T, the compressibility β_T, which relates to κ as $\rho k_B T\beta_T = \kappa$ at $N \rightarrow \infty$, is a weakly increasing function of temperature.

3. Results of Numerical Simulations

We have previously proposed[25] two plausible scenarios to explain inequality 2. The first mechanism was based on the observation that the density of the first hydration layer drops with increasing temperature, and the variance of the number of first-layer waters increases. Both trends point to the formation of a high-temperature hydrophobic interface characterized by enhanced fluctuations of the water density in the first solvation layer.[79,80] The second mechanism anticipated fluctuations of the polarized (ferroelectric) shell induced by low-frequency protein motions with their amplitudes enhanced above T_{tr}. Since long-ranged dipolar forces produce little effect on the interfacial density profile,[81] these two mechanisms can be viewed as essentially uncoupled. As described above, we currently favor the second scenario and present new simulation results and data analysis in support of this mechanism.

Before going into the details, we note that density fluctuations of water at the protein surface, and a hydrophobic surface in general, do not develop an amplitude necessary to explain the observed variances of the electrostatic potential. Indeed, the width of the interfacial region where density fluctuations are active increases slowly with the solute size, as the logarithm of the radius,[82] and does not exceed 0.3 nm for the size magnitude of the protein studied here.[43] Moreover, the compressibility of the first solvation shell is, in fact, lower than that of bulk water. The normalized variance $\kappa^I = \langle(\delta N^I)^2\rangle/\langle N^I\rangle$ (N^I is the fluctuating number of waters in the first solvation layer) increases with rising temperature (Figure 3) but never reaches the level reported by Mittal and Hummer[43] for bulk water. Despite the chemically heterogeneous interface, water molecules are, on average, more constrained in the first solvation layer of a protein than in the bulk.[83−85] This statement applies to high temperatures, since the relation between surface and bulk dynamics is reversed at low temperatures, preventing water crystallization.[86,87] However, for the high-temperature regime mostly studied here, it seems unlikely that translations of waters in and between the hydration layers can produce the breadth of the electrostatic noise recordered from MD trajectories.[25]

3.1. Simulation Protocol. We present here the results of NVT, NPT, and NVE simulations of hydrated plastocyanin with two sizes of the simulation box including $N_s = 5886$ and 21 076 waters to study the effect of the hydration level on the electrostatic observables. In addition, we mutated the wild type (WT) plastocyanin to introduce more charged groups at the surface and thus break up the extended hydrophobic patches

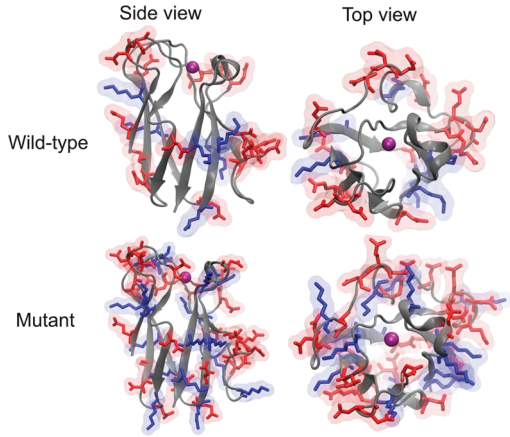

Figure 4. Comparison of the surface charge distribution in the mutant and the wild-type plastocyanin. The PC backbone is given in gray (cartoon representation), and the copper atom is the purple sphere. All ASP/GLU residues are shown in red, and all LYS residues are shown in blue.

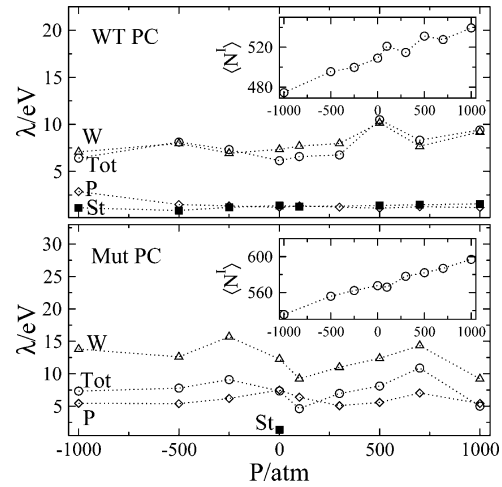

Figure 5. Pressure results for the wild-type (upper panel) and mutated (lower panel) plastocyanin. The points show the total reorganization energy λ^{var} (circles) arising from fluctuations of both the protein and water subsystems, as well as individual protein (diamonds) and water (up triangles) components. The protein−water cross-term (eq 4) is not shown. Solid squares are λ^{St}, and the insets show the pressure dependence of the average number of first-shell waters.

(Figure 4 and Supporting Information). These mutations and the variations of the hydrostatic pressure were carried out to distinguish between the hydrophobicity and ferroelectric shell scenarios. The mutated (Mut) protein was hydrated with $N_s = 6217$ waters. Details of the simulation protocol are given in the Supporting Information. Briefly, AMBER 9.0 package was used to produce MD trajectories with the standard (tinfoil) implementation of the Ewald sums used to treat the Coulomb interactions. To speed up the analysis, the electrostatic interactions were cut off at the half of the box size with the use of the transformation to the standard tinfoil condition according to ref 88 (Tables S1 and S2 in the Supporting Information). This correction is included in the interaction potential V_{0s} of the active-site charges Δq_j with the hydration waters.

In addition to plastocyanin simulations, we have carried out simulations of two other globular proteins, lysozyme and ubiquitin (see Supporting Information for the details of the simulation protocol). These two proteins do not carry redox activity and, therefore, are not used for the reorganization energy calculations. The statistics and dynamics of the dipolar fluctuations of their hydration shells are distinctly different from the redox-active plastocyanin, and these data are used in analyzing the origins of the non-Gaussian electrostatics found for the latter.

3.2. Dependence on Hydrostatic Pressure. Hydrostatic pressure in NPT simulations was varied with the goal of testing the effects of weak dewetting[89] and related enhanced density fluctuations[79] on the protein electrostatics. Both positive and negative hydrostatic pressures were studied, with the latter range (existing in metastable liquids[90,91]) explored given that surface dewetting is enhanced at these conditions.[89] The results of NPT simulations for the wild-type and mutant proteins are shown in Figure 5. The overall outcome is little sensitivity, within simulation uncertainties, of λ_s (either from the Stokes shift or the variance) to hydrostatic pressure; λ_s^{var} increases with increasing pressure, in accord with the increasing number of first-shell waters (insets in Figure 5).

Both the water and protein components of λ^{var} increase in their magnitudes for the mutated compared to the wild-type protein (Figure 5). These trends are consistent with a larger density of surface partial charges for the mutated protein, producing a denser hydration layer with stronger fluctuations of the electrostatic potential. The overall reorganization energy λ^{var} is, however, not that different between the two forms of the protein because of a negative compensating contribution from the cross term, λ_{sp}^{var}, which makes the total reorganization energy of the mutant at some pressure points even lower than the protein and water components separately.

3.3. Formation of the Ferroelectric Water Shell. The first and second cumulants of the dipole moment of waters in the first shell and in the entire simulation box are listed in Table 1 (the pressure dependence of the dipole moments can be found in Tables S3 and S4 in the Supporting Information). The first hydration shell is defined as the water layer of thickness 2.87 Å surrounding the van der Waals surface of the protein. The values obtained for plastocyanin do not depend much on the statistical ensemble (NVE, NVT, and NPT) used in simulations and are also little sensitive to the electrostatic surface mutations, except for the variance of the first-shell dipole, which is smaller in the stiffer hydration shell of the mutant. A significant difference, however, exists between the first-shell dipolar fluctuations of plastocyanin and two non-redox proteins, lysozyme and ubiquitin, studied here. The variances of first-shell dipoles of these proteins are much smaller than that for plastocyanin, implying that the local polarities of their hydration shells are much lower.

Both cumulants $\langle M_s \rangle$ and $\langle (\delta M_s)^2 \rangle^{1/2}$ scale as the square root of the number of waters $N_s^{1/2}$ and, therefore, cannot be compared between different systems. The ratio $\kappa_G = (\langle (\delta M_s)^2 \rangle^{1/2})/\langle M_s \rangle$ is, however, close to $\kappa_G = (3\pi/8)^{1/2} = 1.09$, expected for the isotropic Maxwell distribution for all proteins studied here. For the first-shell dipole $\mathbf{M}_s^I$ of plastocyanin, this ratio, $\kappa_G \simeq 1.14$, reflects a highly anisotropic distribution of the first-shell dipole along the direction of the protein dipole, $\hat{\mathbf{e}}_p = \mathbf{M}_p/M_p$. The corresponding distribution function $P(M_{||})$ of the parallel projection $M_{||} = \mathbf{M}_s^I \cdot \hat{\mathbf{e}}_p$ strongly deviates from the isotropic Maxwell distribution, but at the same time is symmetric in respect to the inversion $M_{||} \rightarrow -M_{||}$ (Figure 6). This nematic symmetry suggests that the anisotropy of $\mathbf{M}_s^I$ is most likely caused by the elongated shape of the protein and not by the pinning field of the protein dipole, which would create an inversion anisotropy. The distribution function, $P(M_{||})$, is not significantly affected by the increase of the overall number of waters in the simulation cell from $N_s = 5886$ to 21 076 (cf. solid to dashed lines in Figure 6), although it is somewhat sharper in the NVE than in the NPT protocol. Nevertheless, these

TABLE 1: Dipole Moments (D) of the Hydration Shell and Protein at 300 K and 1 atm[a]

system	$\langle M_s^l \rangle$	$\langle (\delta M_s^l)^2 \rangle^{1/2}$	$\langle M_s \rangle$	$\langle (\delta M_s)^2 \rangle^{1/2}$	$\langle M_p \rangle$	$\langle (\delta M_p)^2 \rangle^{1/2}$	$\langle N^l \rangle$
WT/Ox (NVT, $N_s = 5886$)	414	464	1152	1242	246	127	509
WT/Ox (NPT, $N_s = 21\,076$)	582	662	2564	2737	249	155	510
WT/Ox (NVE, $N_s = 21\,076$)	485	557	2678	2899	239	218	511
Mut/Ox (NPT, $N_s = 6217$)	316	389	1227	1319	328	223	568
Ub (NVE, $N_s = 27\,918$)	48	50	996	1074	256	30	334
Lys (NVE, $N_s = 27\,673$)	77	71[b]	950	1055	150	38	468
Lys (NVT, $N_s = 27\,673$)	67	69	824	893	162	73[c]	464
Lys (NPT, $N_s = 27\,673$)	67	65	835	904	172	117	459

[a] The data are obtained for wild-type (WT) and mutated (Mut) plastocyanin (PC) in oxidized (Ox) redox state and for lysozyme (Lys) and ubiquitin (Ub) proteins. NVE, NVT, and NPT denote the statistical ensembles used in the simulation protocol. The last column lists the average number of waters in the first solvation layer, $\langle N^l \rangle$. [b] The Kirkwood factor of the first hydration layer of lysozyme is 1.95. A somewhat lower value of 1.45 was reported for TIP3P waters in the first solvation layer of myoglobin (Glass et al. *J. Chem. Theory Comput.* **2010**, *6*, 1390). [c] Previous NVT simulations of lysozyme in SPC/E water (Smith et al. *J. Phys. Chem.* **1993**, *97*, 2009) reported $\langle (\delta M_p)^2 \rangle^{1/2} = 64$ D.

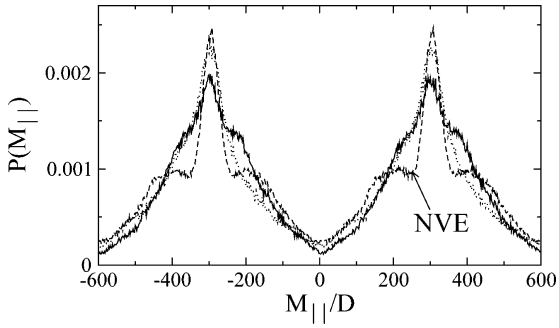

Figure 6. Distribution function $P(M_{||})$ of the parallel projection $M_{||} = \mathbf{M}_s^l \cdot \hat{\mathbf{e}}_p$ of the first-shell water dipole on the direction of the protein dipole $\hat{\mathbf{e}}_p = \mathbf{M}_p/M_p$. The solid line refers to $N_s = 5886$ waters in the simulation box; the dashed lines represent $N_s = 21\,076$ (NPT). The results of the NVE simulations with the same number of particles are also shown. The symmetry with respect to inversion $M_{||} \rightarrow -M_{||}$ indicates that the water shell is not pinned by the electric field of the protein dipole.

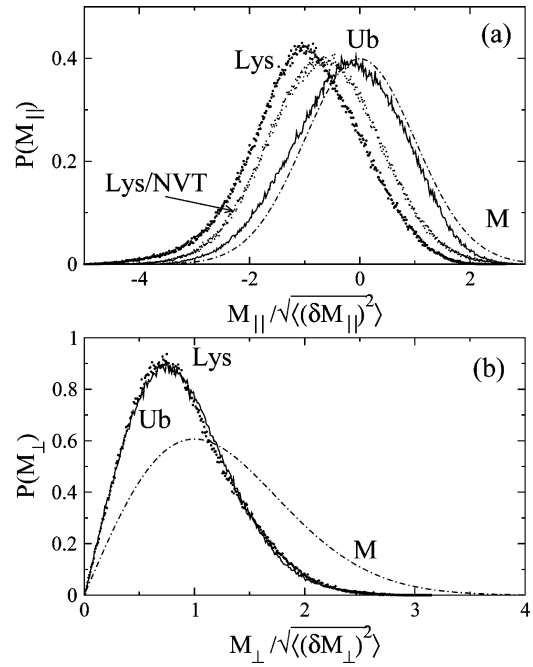

Figure 7. Distributions functions $P(M_{||,\perp})$ of parallel, $M_{||}$ (a), and perpendicular, $M_\perp$ (b), projections of the first-shell dipole on the protein dipole of lysozyme (Lys, points) and ubiquitin (Ub, solid lines). The distribution in panel a marked as Lys/NVT refers to the NVT simulation of lysozyme; all other distributions are from the NVE simulations. The dashed−dotted lines in both panels refer to the isotropic Maxwell distribution (M).

results testify to a relatively low sensitivity of the first-shell structure to the size of the simulation box.

We found that both the dynamics and statistics of the first-shell dipole moment of lysozyme and ubiquitin are distinctly different from plastocyanin. There are noticeable, although much smaller, deviations of the distribution functions $P(M_{||})$ and $P(M_\perp)$ ($M_\perp$ is the component of $\mathbf{M}_s^l$ perpendicular to $\hat{\mathbf{e}}_p$) from the Maxwell distribution (Figure 7). A part of it comes from insufficient statistical sampling. The dynamics of $\mathbf{M}_s^l(t)$ for these proteins are extremely slow, with characteristic relaxation times of 1600 ps (Lys) and 400 ps (Ub) (Figure 8). As a result, $\mathbf{M}_s^l(t)$ of lysozyme and ubiquitin do not average to zero on the 25 ns length of the MD trajectory (Figure 7). The nonvanishing first-shell dipole $\langle \mathbf{M}_s^l(t) \rangle$ of ubiquitin is smaller than of lysozyme, and the distribution $P(M_{||})$ is closer to Maxwellian. However, the first hydration shells of both these proteins will appear ferroelectric on a subnanosecond observation window.

We have also found that the dipolar dynamics of both lysozyme and ubiquitin are significantly faster in NVT/NPT simulations as compared with the NVE protocol (see Figure S1 in the Supporting Information), which is most likely an artifact of the thermostats employed in the NVT/NPT simulations. As a result of faster relaxation, the distribution function, $P(M_{||})$, of Lys obtained in the NVT ensemble shifts closer to the Maxwell distribution (Figure 7). Note that we found no such ensemble effects on the dynamics of plastocyanin, which are much faster than those of lysozyme and ubiquitin (see below).

3.4. Propagation of the Shell Polarization into the Bulk. Since the statistics of electrostatic fluctuations are strongly influenced by thermal motions of the ferroelectric cluster, the question of its spatial extent into the bulk water becomes critical for the development of the physical picture of the water−protein interface. To study this aspect of the dipolar polarization, we have calculated the dipolar properties originating from the waters located within the layer of thickness r from the protein surface. A water molecule is assigned to the layer if the separation of its oxygen atom from the nearest protein atom is within the r distance. The results for the water shell dipole are summarized in Figure 9, where the average dipoles are given in panels a and c and the variances are shown in b and d.

Both the average dipole moment and its variance increase with the layer thickness r (Figure 9a−b). This increase comes from the growing number of waters in the shell, since the average dipole moment per water molecule at distance r, $\langle m_s(r) \rangle = dM_s(r)/dN_s(r)$, actually decays with r (Figure 9c). A similar trend is seen for the distance-dependent Kirkwood factor, $g_K(r) = \langle \mathbf{M}_s^2(r) \rangle / (\langle N_s(r) \rangle m_s^2)$, where $m_s = 2.35$ D is the dipole moment of a TIP3P water molecule (Figure 9d). The statistics of the shell dipole are little affected by temperature. Both the average

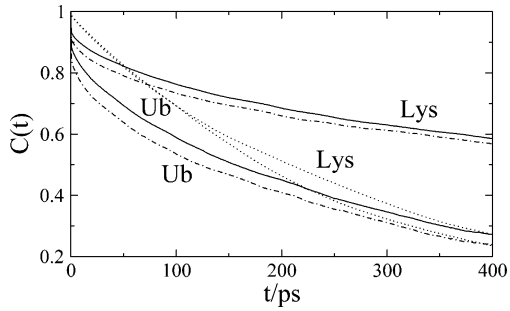

Figure 8. Normalized self-correlation functions of dipole moments of lysozyme (Lys) and ubiquitin (Ub). The solid lines show the correlation functions $C_s^I(t)$ of the first-shell dipole; the dashed−dotted lines show the correlation functions of the first-shell unit vector $\hat{\mathbf{e}}^I(t) = \mathbf{M}_s^I(t)/M_s^I(t)$. The dotted lines refer to the correlation function $C_s(t)$ of the entire dipole moment of the simulation box.

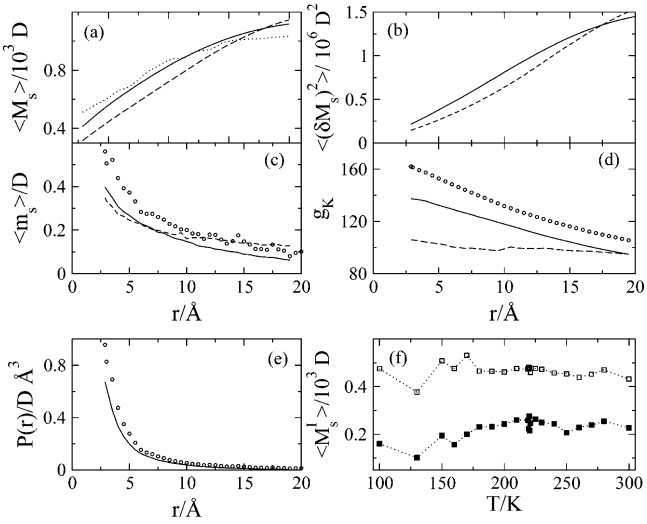

Figure 9. Dependence of the water dipole moment on the thickness of the water shell (a−e) and the variation of the first-shell dipole with temperature (NVT simulations,[25] panel f). All results are from MD simulations of PC. The dipole moment per water molecule residing at distance r from the protein surface $\langle m_s(r)\rangle = dM_s(r)/dN_s(r)$ is shown in panel c, and the distance-dependent Kirkwood factor, in panel d. The distance-dependent dipolar polarization $P(r) = dM_s(r)/(4\pi r^2\, dr)$ is shown in panel e. Panel f shows the average ($\langle M_s^I\rangle$, open squares) and variance ($\langle(\delta M_s^I)^2\rangle$, closed squares, in 10^6 D^2) of the first-shell dipole vs temperature. The solid and dashed lines correspond to the wild type and mutant proteins, respectively, obtained from simulations with smaller simulation cells ($N_s = 5886$ (WT) and 6217 (Mut)). Open circles refer to simulations of WT/Ox PC with $N_s = 21\,076$ waters in the simulation cell. The dotted line in panel a shows the water dipole moment around WT/Ox PC at 150 K.

and the variance of $\mathbf{M}_s^I$ are almost independent of temperature (Figure 9f), and $M_s(r)$ is nearly the same at high and low temperatures (cf. dotted and solid lines in Figure 9a). The hydration shell also becomes slightly more dense when the number of waters in the simulation box is increased from $N_s = 5886$ to $N_s = 21\,076$. This is reflected by higher $\langle m_s(r)\rangle$ (Figure 9c) and $g_K(r)$ (Figure 9d). Nevertheless, the polarization density of the water shell $P(r) = dM_s(r)/(4\pi r^2 dr)$ remains fairly consistent between the two simulations (cf. solid line with points in Figure 9e) and decays approximately as $1/r^2$ into the bulk. Virtually no polarization is detected beyond $r \simeq 10$ Å (Figure 9c), which incorporates ≃2300 waters into the ferroelectric cluster.

The variance reorganization energy $\lambda_s^{var}(r)$ can also be calculated by counting the fluctuations of the Coulomb potential arising from a given water layer. No correction for the cutoff

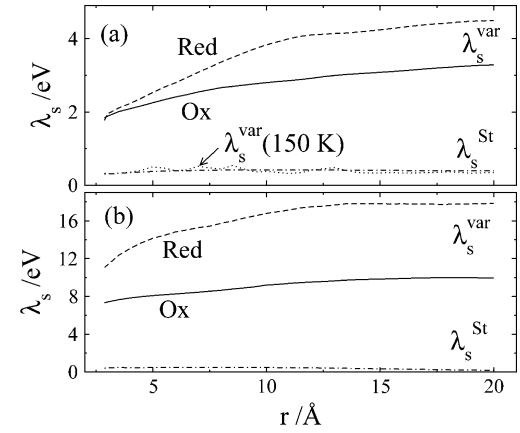

Figure 10. Reorganization energies $\lambda_s^{var}(r)$ and $\lambda_s^{St}(r)$ calculated from the water shell of thickness r around the wild-type plastocyanin (a) and its mutant (b). "Ox" and "Red" specify the oxidation states. The dotted line in panel a shows $\lambda_s^{var}(r)$ of PC/Ox at $T = 150$ K.

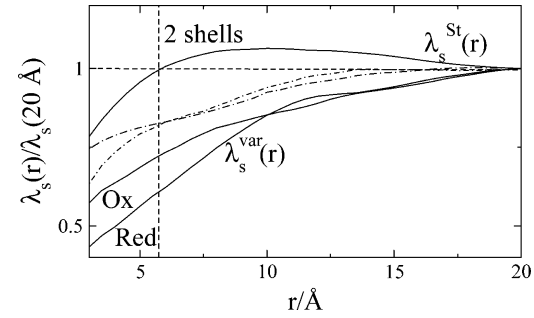

Figure 11. Reorganization energies $\lambda_s^{var}(r)$ and $\lambda_s^{St}(r)$ obtained for Red and Ox states of wild-type plastocyanin (solid lines). The dashed−dotted lines show $\lambda_s^{var}(r)$ for the mutant protein. All parameters are calculated for a shell of waters inside the thickness r from the protein surface and reduced to their corresponding values at $r = 20$ Å. The vertical dashed line indicates the thickness of two solvation shells around the protein within which $\lambda_s^{St}(r)$ nearly reaches its bulk value. The data are obtained from NPT simulations with $N_s = 5886$ waters in the simulation box.

of the interaction potential is taken in this case. These results are therefore only qualitative and are meant to show the characteristic length on which the variance of electrostatic fluctuations builds up. The functions $\lambda_s^{var}(r)$ obtained in two oxidation states of the protein basically follow the trend seen for the shell water dipole, extending the radius of their convergence to about five solvation layers from the protein surface. Nevertheless, at least half of $\lambda_s^{var}(r)$ is produced by fluctuations of the first solvation layer alone, again emphasizing the interfacial nature of the reorganization energy λ_s^{var} (eq 7). Further, the water reorganization energy of the mutant is much higher than that of the wild-type protein, reaching a gigantic magnitude comparable in the past only to the report by Tan et al.[68] It appears that more tightly bound hydration shells of the mutant produce more electrostatic noise, at the same time leading to a stronger compensation between protein and water fluctuations in the overall reorganization energy λ^{var} (Figure 5 and Tables S1 and S2 in the Supporting Information).

The Stokes shift reorganization energy λ_s^{St} is much lower than λ_s^{var} and is comparable to the latter only at low temperatures below T_{tr} (cf. dashed−dotted and dotted lines in Figure 10a). Importantly, $\lambda_s^{St}(r)$ does not share the long-range character of $\lambda_s^{var}(r)$ and mostly reaches its bulk value within the first two solvation layers (Figure 11). Therefore, the dramatic distinction in the magnitudes of λ_s^{St} and λ_s^{var} is also reflected in different length scales involved. Although λ_s^{St} is clearly a short-range

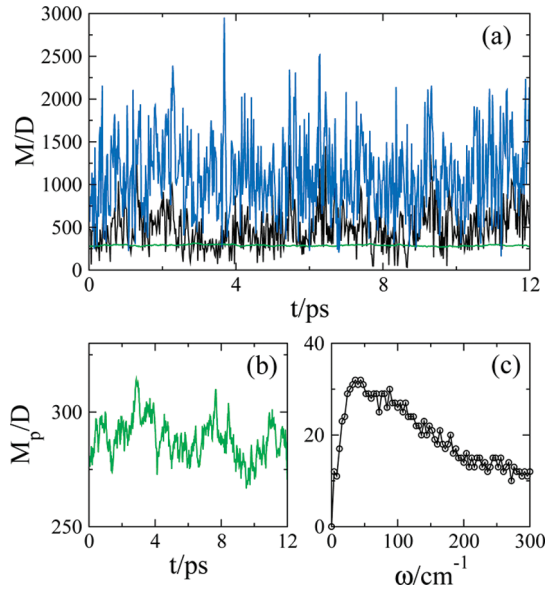

Figure 12. Trajectories of the dipole moment of the protein $M_p(t)$ (green), first-shell water $M_s^I(t)$ (black), and total hydration water $M_s(t)$ (blue) from NPT simulations of plastocyanin. Panel (b) shows a magnified protein trajectory $M_p(t)$,, and panel c shows the density of normal-mode vibrations of the protein.

property, as is typical for solvation of small molecules, large increase in λ_s^{var} at $T > T_{tr}$ originates from a collective mode linked to long-ranged fluctuations of the shell dipole moment. This mode dynamically freezes below T_{tr}, and $\lambda_s^{var}(r)$ not only becomes close to $\lambda_s^{St}(r)$ in magnitude, but also loses its long-range length scale.

3.5. Shell Dynamics. We now turn to the dynamics of the ferroelectric water shell. This issue is critical for our entire discussion since the results shown in the previous sections naturally raise a number of questions: (i) Why have any of the long-ranged dipolar structures not been detected by X-ray crystallography and NMR?[84] and (ii) Why was the spatially extended water polarization observed on a very short time scale of the terahertz dielectric response[27] and has it not been detected by conventional dielectric spectroscopy[20] at lower frequencies?

To address these questions and get a better grasp of the nature of the dynamical transition in the spectrum of electrostatic fluctuations, we have looked at the dynamics of three relevant dipole moment vectors: dipole moment of the protein $\mathbf{M}_p(t)$, dipole moment of the first-shell waters $\mathbf{M}_s^I(t)$, and dipole moment of all water molecules in the simulation box $\mathbf{M}_s(t)$. These observables are compared with the dynamics of the Coulomb interactions of the active site with the protein and water thermal bath.

The trajectories of all three dipole moment magnitudes of hydrated plastocyanin are shown in Figure 12a−b. All dipoles experience rapid fluctuations on a time scale of ≃1 ps, consistent with both the time scale of hydrogen-bond dynamics in water[70,71] and the peak of the normal-mode density of states of plastocyanin (Figure 12c). This type of vibrational density of states is typically observed for hydrated proteins.[92,93] The physical picture arising here is that of low-frequency vibrations of the protein pushing hydration water and producing amplified fluctuations of the ferroelectric shell, which follows essentially adiabatically the protein motions. These vibrations also include motions of α-helices with the corresponding fluctuations of their large dipoles.

This picture is supported by the time correlation functions shown in Figure 13. The time self-correlation function of the

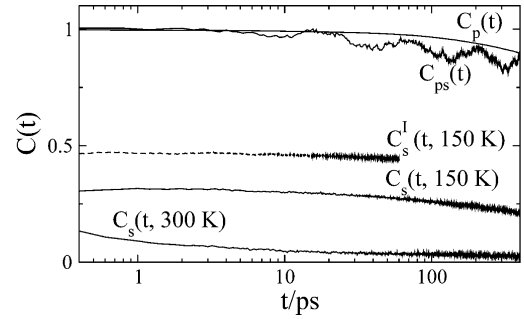

Figure 13. Normalized time correlation functions of the protein (p) and water (s) dipole moments. Also shown are the correlation function of the first-shell water dipole, ($C_s^I(t)$), at 150 K and the cross correlation function of the protein and water dipole moments (ps).

protein dipole $C_p(t) = \langle \mathbf{M}_p(t) \cdot \mathbf{M}_p(0) \rangle / \langle M_p(0)^2 \rangle$ shows a very slow exponential decay with the time scales from 2.8 ns for N_s = 5886 to 6.4 ns for N_s = 21076. This relaxation is typically assigned to protein tumbling.[94] The decoherence of water motions, represented by $C_s^I(t) = \langle \mathbf{M}_s^I(t) \cdot \mathbf{M}_s^I(0) \rangle / \langle M_s^I(0)^2 \rangle$ and $C_s(t) = \langle \mathbf{M}_s(t) \cdot \mathbf{M}_s(0) \rangle / \langle M_s(0)^2 \rangle$, is much faster, on a 0.3−0.5 ps time scale. These dynamics have also been recordered by spectroscopic techniques and were assigned to the peptide−water hydrogen-bond motions.[93] Most of the water's correlation functions, $C_s(t)$ and $C_s^I(t)$, decay on this very short time scale, followed by ∼5% amplitude with a relaxation time scale of ≃100 ps.

In contrast, the cross-correlation function $C_{ps}(t) = \langle \mathbf{M}_p(t) \cdot \mathbf{M}_s(0) \rangle / \langle \mathbf{M}_p(0) \cdot \mathbf{M}_s(0) \rangle$ follows the protein relaxation for at least ≃100 ps, and the same is true for the cross-correlation of $\mathbf{M}_p^I(t)$ and $\mathbf{M}_s^I(t)$ (not shown in Figure 13). The polarization of the water cluster therefore follows adiabatically the protein's motions. The ferroelectric shell surrounding the protein is truly elastic with a characteristic ≃1 ps relaxation time detected by terahertz spectroscopy, in contrast to the protein dipole nearly frozen on that time scale.

The dynamics of the water shell are not much affected by the change of the number of waters from N_s = 5886 to 21 076; the results of analyzing the larger simulation box are summarized in Table 2. The dynamics of $\mathbf{M}_s^I(t)$ are also very close to that of the corresponding unit vector $\hat{\mathbf{e}}^I(t) = \mathbf{M}_s^I(t)/M_s^I$, indicating that most of the dipolar relaxation occurs by rotations of $\mathbf{M}_s^I(t)$ instead of its magnitude fluctuations (which are also present; Figure 12). Also shown in the table are the relaxation times of the number $N^I(t)$ of first-shell waters calculated from $C_N(t) = \langle \delta N^I(t)\ \delta N^I(0) \rangle / \langle (\delta N^I(0))^2 \rangle$. The water exchange between first and second shells occurs on a time scale of 2 ps, consistent with previous NMR reports.[84]

What happens with the dipole moment dynamics with lowering temperature is illustrated in Figure 13. The slow components of $C_s^I(t)$ and $C_s(t)$ increase both in amplitude and in the relaxation time with lowering temperature. For instance, the slow, 80−150 ps, relaxation component of $C_s^I(t)$ is almost negligible (4−7%) at 300 K, but increases to 30−50% when the temperature drops to 150 K. In addition, the relaxation time increases to 1.6 ns.

As we have mentioned above, the dynamics of plastocyanin are almost identical in the NVE and NVT ensembles (Table 2), although the former generally offers a better protocol for dynamics simulations.[95] In contrast, the dipolar dynamics of lysozyme and ubiquitin, much slower even at high temperatures, are sensitive to the ensemble used (Figure S1 in the Supporting Information). The first-shell dipoles of lysozyme and ubiquitin

TABLE 2: Relaxation Times (τ, ps) and Relative Amplitudes (A) of the Normalized Time Correlation Functions of Water Dipole, the Number of First-Shell Waters, and Electrostatic Interactions Obtained from NVT (20 ns)/NVE (25 ns) Simulations of WT/Ox Plastocyanin with $N_s = 21076$ Waters in the Simulation Box

observable	ensemble	relaxation times and amplitudes			
$\hat{\mathbf{e}}^I$	NVT	τ_e^I	0.03	1.5	85
		A_e^I	0.81	0.12	0.07
	NVE	τ_e^I	0.08	3.2	140
		A_e^I	0.85	0.10	0.05
$\mathbf{M}_s^I$	NVT	τ_M^I	0.04	1.4	85
		A_M^I	0.79	0.14	0.07
	NVE	τ_M^I	0.08	2.1	139
		A_M^I	0.83	0.11	0.06
$\mathbf{M}_s$	NVT	τ_M	0.006	0.62	4.8×10^8
		A_M	0.75	0.21	0.04
	NVE	τ_M	0.1	3.1	1203
		A_M	0.92	0.05	0.03
N^I	NVE	τ_N^I	0.53	41	2593
		A_N^I	0.80	0.15	0.05
V_{0s}[a]	NVE	τ_p	0.35	46	650
		A_p	0.23	0.12	0.65
V_{0p}[a]	NVE	τ_w	0.25	11	548
		A_w	0.39	0.21	0.40
$V_{0,ps}$[b]	NVE	τ_{pw}	0.62	9.5	539
		A_{pw}	0.22	0.27	0.51

[a] Coulomb interaction energy of the active site with the partial charges of water, V_{0s}, and protein, V_{0p}. [b] Relaxation parameters of the cross-correlation function between Coulomb interaction energies with protein and water.

do not average to zero on the 25 ns length of the simulation trajectory. The slow components make ~75% of $C_s^I(t)$ for both proteins, with the relaxation times of 1600 ps (Lys) and 400 ps (Ub) (Figure 8). Nevertheless, for all protein studied, the correlation functions of the unit vectors $\hat{\mathbf{e}}^I(t)$ are very close to the $C_s^I(t)$ functions, indicating that the dipolar relaxation occurs in all cases by rotations of the dipole moment $\mathbf{M}_s^I(t)$.

It seems plausible that a nuclear mode responsible for the slow portion of the dipole relaxation is the main contributor to the dynamics of electrostatic fluctuations and the dynamical freezing of the reorganization energy λ_s^{var} below T_{tr} (Figure 1d). This is suggested by the dramatic difference in the relaxation patterns of the dipole moment and the electrostatic potential of plastocyanin. In contrast to protein and water dipoles, which relax on quite distinct time scales, the time correlation functions of the Coulomb interaction energies $V_{0p}(t)$ and $V_{0s}(t)$ are fairly close to each other (Figure 14).

The relative weights of the fast and slow relaxation components are also remarkably different between the dipole moment and Coulomb interaction energies. Most of the water dipole around plastocyanin relaxes on a really short time scale (Figure 13). In contrast, the slow relaxation tail of 0.5−2 ns, barely seen in functions $C_s(t)$ and $C_N(t)$ (Table 2), becomes a dominant component of the relaxation functions $C_V(t) = \langle \delta V_{0a}(t)\, \delta V_{0a}(0)\rangle / \langle (\delta V_{0a}(0))^2\rangle$ calculated for interactions of the active site with the protein (a = p) and water (a = w). This long-time relaxation also amounts to ~60% of the variance reorganization energy λ_s^{var}. Not surprisingly, this slow relaxation freezes in at low temperatures, eliminating, on a fixed observation window, much of the breadth of the electrostatic noise observed at high temperatures (Figure 1d). Consistent with the highly correlated dynamics of $V_{0p}(t)$ and $V_{0s}(t)$, there is a substantial compensation between the positive protein, λ_p^{var}, and water, λ_s^{var}, components of λ^{var} and a negative cross-correlation term λ_{sp}^{var} (Figure 5 and Table 3).

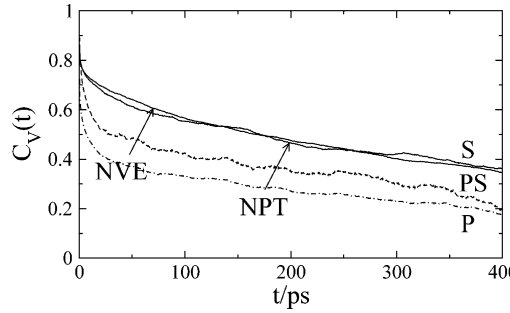

Figure 14. Normalized Stokes shift correlation function $C_V(t) = \langle \delta V_{0a}(t)\ \delta V_{0a}(0)\rangle / \langle (\delta V_{0a}(0))^2\rangle$, a = s, p, obtained for the Coulomb interaction energy of the active site with the protein (p, dashed−dotted line) and water (s, solid lines). The dashed line line marked as "ps" refers to the normalized cross-correlation function between protein and water Coulomb energies. The water component of the Stokes shift correlation function is shown for NPT and NVE simulations (N_s = 21 076); the rest of the data are from the NVE trajectory.

TABLE 3: Components of λ^{var} and λ^{St} (eV) from Coulomb Interactions with the Protein (p) and Water (s)

system	λ^{var}	λ_s^{var}	λ_p^{var}	λ_{sp}^{var}	λ^{St}	λ_p^{St}	λ_s^{St}
WT/Ox (NPT, N_s = 5886)	8.4	8.6	1.2	−1.4	1.07	0.60	0.47
WT/Ox (NVT, N_s = 5886)	7.7	5.6	1.6	0.5	0.69	0.29	0.40
Mut/Ox (NPT, N_s = 6217)	7.0	11.7	7.5	−12.2	1.37	0.88	0.49
WT/Ox (NPT, N_s = 21 076)	5.2	7.2	2.5	−4.5			
WT/Ox (NVT, N_s = 21 076)	7.2	6.7	1.4	−0.9			
WT/Ox (NVE, N_s = 21 076)	7.6	7.2	1.5	−1.1			

4. Discussion

The current view of the dynamics of the protein−water interface highlights the primary role of water translations and corresponding hydrogen-bond fluctuations. These fluctuations lubricate and enhance the mobility of protein's surface groups (e.g. amino acid side chains), driving anharmonic protein fluctuations above the temperature T_{tr} of the dynamical transition. Density modes, and corresponding relaxation via surface diffusion, are relatively short-ranged and thus local. What we report here carries quite a different meaning. We found a (first-order[25]) transition of a mesoscopic layer of waters surrounding the protein to an orientationally cooperative (ferroelectric) cluster with a very substantial average magnitude of its dipole moment. The polarization mode driving this transition involves hundreds of water molecules coupled in their rotational motions by long-ranged Coulomb interactions. The concept of slaving the protein dynamics by water[5] gains a new dimension in this picture. It is not that single-particle dynamics of individual interfacial waters that slave conformational protein dynamics, but concerted fluctuations of a large polarized cluster comparable in size to the size of the protein itself. When, with increasing temperature, the characteristic relaxation time of the principal polarization mode appears in the observation window of a laboratory/numerical experiment, one observes a kinetic transition leading to a dramatic rise in the breadth of electrostatic fluctuations and magnitudes of atomic displacements (Figure 1).

The appearance of a new mesophase reveals itself in the breakdown (eq 2, Table 3) of the linear response relations between electrostatic observables obtained from statistical averages and variances. These observations pose two major

questions: (i) Does the presence of a protein solute induce the formation of the cooperative ferroelectric cluster in its solvation shell? and (ii) Whether the elastic stress of this cluster produced by the protein conformations/vibrations is responsible for the non-Gaussian statistics of the electrostatic fluctuations? A partial answer to the first question may be sought from simulations of model dipolar fluids.[96,97] A transition to a bulk liquid ferroelectric was found in these systems at a dipolar strength of about $\sim\beta m^2/\sigma^3 \simeq 7$ (m is the solvent dipole moment and σ is the effective diameter).[98,99] A macroscopic ferroelectric phase has, of course, not been observed for bulk water. However, the presence of a large solute might lower the local free energy minimum of the ferroelectric phase, positioned above the paraelectric minimum of bulk water, toward a stable ferroelectric subensemble. The reduced dipole moment of water, $\beta m^2/\sigma^3$, is $\simeq$5.8 for the TIP3P force field and $\simeq$10 based on more recent ab initio estimates.[100] This value falls rather close to the critical value of ferroelectric transition found in simple dipolar fluids, and one can hypothesize that this mesophase can be stabilized within a subensemble of the hydration shell waters.

The question of how generic the ferroelectric shell enveloping the protein can be obviously needs further studies. What we have found from this and some previous studies is that enhanced dipolar fluctuations of the water shell have been observed for redox-active proteins[58,66,68,101] but are significantly reduced for ubiquitin and lysozyme (Table 1), which are not redox-active in natural systems. What is a set of key parameters of the protein fold/charge distribution that are responsible for very large values of $\langle(\delta M_s^I)^2\rangle$ is not clear, but Table 1 indicates that the vibrational modulation of the protein dipole might be an important indicator. One can speculate that the modulation of the protein electrostatics by low-frequency conformational modes might be behind a large breadth of the electrostatic noise observed for redox-active proteins.

A connection between the protein rigidity[103] and the dipole moment fluctuations is in line with the current interpretation of the dynamical transition in proteins.[5] One can extract the conformational component of the mean-square displacement of myoglobin iron $\langle\delta x^2\rangle_c$ in Figure 1a by subtracting the linearly extrapolated low-temperature component due to protein vibrations. It was then shown that the corresponding Lamb−Mössbauer factor $f_c = \exp[-k_0^2\langle\delta x^2\rangle_c]$ (k_0 is the wavevector of the gamma radiation) can be exceptionally well reproduced by the dipole moment variance[5]

$$f_c = 1 - \langle(\delta\mathbf{M})^2\rangle_{obs}/\langle(\delta\mathbf{M})^2\rangle \qquad (9)$$

Here, $\mathbf{M} = \mathbf{M}_p + \mathbf{M}_s^I$ is the dipole moment of the protein and its first hydration layer. Further, the nonergodic average $\langle...\rangle_{obs}$ is carried out on the times shorter than the instrumental time of $\tau_{obs} = 140$ ns. Equation 9 shows that configurational, anharmonic flexibility of the protein detected at $T > T_{tr}$ can be gauged by the dipole moment fluctuations.

The dynamics and statistics of the shell dipole moment turned out to be protein-specific, as indicated by a dramatic distinction between the redox-active plastocyanin and redox-inactive lysozyme and ubiquitin (cf. Figure 6 and Figure 7). Although the distributions of the first-shell dipoles of the latter two proteins are qualitatively close to the prediction of the Maxwell distribution, there is a qualitative difference in the case of plastocyanin. The hydration shell around this protein breaks into oppositely oriented dipolar domains with a resulting anisotropy of the dipole moment distribution function.

TABLE 4: Reorganization Energy λ^{var} (eV) and the non-Gaussianity Parameter $\lambda^{var}/\lambda^{St}$ Obtained from MD Simulations of Hydrated Solutes

system	τ_{sim}/ns[a]	λ^{var}	$\lambda^{var}/\lambda^{St}$	ref
WT/Ox (NPT, $N_s = 5886$)	10	8.4	7.9	
Rhodobacter sphaeroides reaction center (NPT, $N_s = 10\,506$)	10		8−10	101
Four-helix protein/RuDPP cofactors (NPT, $N_s = 5148$)	10	4.8[b]	3.7	58
[4**Fe**−4**S**] ferredoxin (NVE, $N_s = 2782$)	3.3	11.7	8.0	68
Dendrimer/porphyrin (NVE, $N_s = 2000$)	0.1	2.08[c]	2.1[c]	102

[a] The length of the simulation trajectory. [b] Obtained from Table 3 in ref 58. [c] From Figure 6 in ref 102.

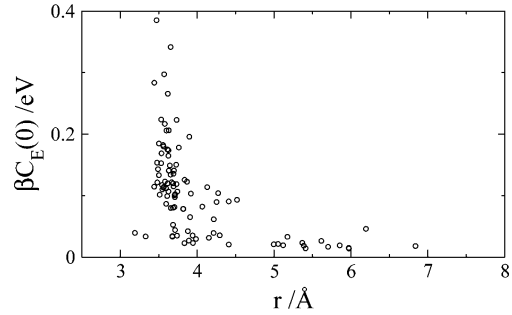

Figure 15. Variance of the interaction energy of the electric field $\mathbf{E}_s$ of hydration waters with the carbonyl dipole of a protein residue: $C_E(0) = \langle(\mathbf{m}\cdot\delta\mathbf{E}_s)^2\rangle$. The variance calculated for different residues of WT/Red plastocyanin is plotted vs the distance from the carbonyl group to the nearest oxygen of water. A dipole moment of $m = 1.78$ D aligned with the C═O bond was placed at each carbonyl to calculate the interaction energy.

Inequality 2 has been recordered by now in numerical simulations of several hydrated solutes.[58,66,68,101,102,104] The results collected from the literature are summarized in Table 4. It is still not entirely clear if a significant upward deviation of the non-Gaussianity parameter $\lambda^{var}/\lambda^{St}$ from unity signifies the appearance of a ferroelectric water cluster. Note that short simulations tend to lose slow dynamics, mainly contributing to λ^{var} (Figure 14), and thus underestimate non-Gaussianity. We also want to emphasize that the last entry in Table 4 is a large nonprotein solute. We have also previously found $\lambda_s^{var}/\lambda_s^{St} \simeq 1.5$ for a small hydrated charge-transfer molecule.[104] It might turn out that non-Gaussian electrostatic fluctuation is a general property of hydration amplified by large solutes.[105]

The long-standing question of the polarity of the protein matrix[106−108] and the protein−water interface[109] becomes somewhat ill-defined in view of our current picture. It has long been recognized that proteins make a highly anisotropic electrostatic environment.[35,106] This observation is additionally illustrated by our mapping of the local polarity of plastocyanin using the variance of the electric field of the water solvent at carbonyl groups of residues distributed throughout the protein matrix (Figure 15). The data are arranged according to the distance from a carbonyl group to the nearest oxygen of water and show a strong inhomogeneity in the electric field fluctuations, which should affect the Stokes shifts probed by fluorophores.[26,29−32]

Even more generally, the breakdown of the linear response approximation and the slow Stokes shift dynamics observed in our simulations require more specific definition of the polarity of the protein−water interface. Although the average electrostatic potential follows the standard expectations of linear solvation models,[64] its variance reflects an effectively much more

polar environment characterized by an intense electrostatic noise. Furthermore, slow relaxation is the main portion of the time correlation function of electrostatic potential, making some of the interfacial nuclear modes dynamically arrested on short observation times. The question of protein polarity thus needs to be addressed not only in regard to the magnitude of the observed response, which itself varies dramatically between the first and second moments, but also in connection with the time window open to observation. The sluggishness of proteins makes them nonpolar on narrow observation times of a few picoseconds and very polar, when fluctuations are concerned, on longer time scales in the nanosecond range.[101] The question of polarity of proteins then strongly depends on what is recordered and how long one has watched. The protein function and stability can then be adjusted through altering the protein fold or surface charge distribution, which will in turn affect either the dynamics or statistics of the interfacial electrostatic fluctuations.

5. Experimental Evidence

The experimental evidence pointing to the existence of ferroelectric clusters around proteins comes from terahertz dielectric measurements, which by now have been done on both neutral[55] and charged[110,111] proteins. The interpretation of the observed dependence of the dielectric absorption on protein's concentration (Figure 1c) requires a much larger effective dipole moment than the one assigned to the protein alone on the basis of its atomic charges.[28] We suggest that this much larger overall dipole is a sum of the protein dipole and the dipole of the ferroelectric cluster enveloping it.

Anomalous terahertz absorption was found to be strongly affected by both the buffer pH[55] and local mutations altering the protein flexibility.[111] Whereas partial unfolding might be the answer to both effects, another possibility is the effect of altering the properties of the polarized water cluster through the ionization state of surface residues. Our current simulations do not support this latter possibility, since neither the statistics nor the dynamics of the ferroelectric dipole are significantly altered by the mutation (Table 1). The dynamical nature of the polarized cluster should be stressed when relating these observations to a laboratory experiment. Charge and structural mutations may shift the relaxation time of the hydration shell out of the experimental frequency windowm thus affecting the measured absorption coefficient.[28]

We found that the amplitude of the slow ($\simeq$0.5−2 ns) relaxation component of the shell dipole moment grows with lowering temperature (Figure 11). This observation offers the possibility to detect the large dipole of the water shell in the gigahertz frequency window of dielectric spectroscopy or depolarized light scattering[112] at low temperatures. Experiments on low-hydration protein powders are, however, unlikely to detect the corresponding polar response, since nonpolar boundary conditions imposed on the hydration shells in powders are likely to eliminate ferroelectric clusters.[97] In addition, water crystallization beyond the first solvation layer[10] will potentially make low-temperature observations problematic. Terahertz spectroscopy of bulk solutions seems to provide the right boundary conditions and observation window, but the interpretation of the results still requires an extensive theory development.[28]

Small-angle X-ray scattering measures the radius of gyration of a hydrated protein typically exceeding the radius from the crystal structure.[113] Since the usual signal is a merged pulse train of a nanosecond length, the radius of gyration is expected to grow with lowering temperature when the slow relaxation of the ferroelectric cluster enters the observation window and increases in the relative amplitude. This trend is, indeed, observed in such measurements,[113] although the experimental resolution might be insufficient for a more detailed picture.

We finally briefly comment on experimental observations of the electrostatic parameters λ^{St} and λ^{var} for redox proteins. These two reorganization energies determine the activation barrier for exchanging electrons between different redox states and also affect the equilibrium redox potential established when the barriers for oxidation and reduction half-reactions become equal. The activation barrier of an electrode process is $(\lambda^{St} + e\eta)^2/(4\lambda^{St})$ in the linear response approximation ($\lambda^{St} = \lambda^{var}$), where η is the electrode overpotential.[114] The activation barrier $\Delta G^{\dagger} = \lambda^{St}/4$ at $\eta = 0$ then gives access to the reorganization energy. Cyclic voltammetry measurements mostly done on redox proteins immobilized on self-assembled monolayers coating electrodes, as well as other techniques,[115,116] have consistently produced very low activation barriers, suggesting values of the reorganization energy $\lambda^{St} = 4\Delta G^{\dagger}$ in the range 0.1−0.4 eV.[117−122] Similar results, $\lambda^{St} \simeq 0.2-0.35$, are reported from Arrhenius slopes of electrode reaction rates[123,124] by assuming $\lambda^{St} = 4\Delta H^{\dagger}$ and thus neglecting the activation entropy. In particular, recent measurements on spinach plastocyanin,[124] the same protein as studied here, yielded the activation enthalpy at equilibrium electrode potential equal to $4\Delta H^{\dagger} = 0.24-0.28$ eV. This magnitude is well below $\lambda^{St} \simeq 0.7-1.2$ eV of the plastocyanin half reaction (Table 3) and of half reactions of other redox proteins reported from previous numerical simulations.[125]

An explanation of this clear discrepancy naturally comes from the notion of non-Gaussian electrostatic fluctuations communicated here. The non-Gaussian noise results in nonparabolic free-energy surfaces of electron transfer,[59] and the standard equations for the activation barrier[69] do not strictly apply anymore. A local harmonic approximation, with two reorganization energies λ^{St} and λ^{var} to characterize, correspondingly the relative shift of two parabolas and their curvature, can be used to estimate the activation free energy if the activation barrier is not too high.[101] When the reorganization energies from the first and second cumulants differ, the activation barrier of an electrode process at $\eta = 0$ becomes $\Delta G^{\dagger} = (\lambda^{St})^2/(4\lambda^{var}) = \lambda^{eff}/4$. The effective reorganization energy experimentally observed in electrode kinetic experiments then becomes

$$\lambda^{eff} = (\lambda^{St})^2/\lambda^{var} \tag{10}$$

With the numbers for WT/Ox PC (NPT) listed in Table 3 one gets $\lambda^{eff} = 0.13$ eV, in the range of values commonly reported by cyclic voltammetry. Given that the reorganization entropy is typically positive and $T\Delta S^{\dagger}/\Delta G^{\dagger} \simeq 0.5$,[104] one can estimate the enthalpy of activation for oxidizing/reducing plastocyanin as $4\Delta H^{\dagger} = 0.2$ eV. This value will increase and become closer to the experimentally reported magnitude of 0.24−0.28 eV[124] when the internal reorganization energy, $\simeq$0.1 eV,[126] of the active site is additionally taken into account. From this analysis, one can suggest that anomalously low reorganization energies in electrochemical kinetics of proteins[117−124] and in a number of electronic transitions characterized by low reaction free energies[115,116,127−129] may result from the application of the Gaussian activation formulas to where non-Gaussian fluctuations determine the activation thermodynamics.

Acknowledgment. This research was supported by the NSF (CHE-0910905). We are grateful to Dor Ben-Amotz for many

useful comments on the manuscript. CPU time was provided by ASU's Center for High Performance Computing and by a number of allocations through the TeraGrid Advanced Support Program (TG-MCB080071, TG-MCB080116N, TG-ASC090088).

Supporting Information Available: Additional information as noted in text. This material is available free of charge via the Internet at http://pubs.acs.org.

References and Notes

(1) Parak, F. G. *Rep. Prog. Phys.* **2003**, *66*, 103.
(2) Fenimore, P. W.; Frauenfelder, H.; McMahon, B. H.; Young, R. D. *Proc. Natl. Acad. Sci.* **2004**, *101*, 14408.
(3) Caliskan, G.; Briber, R.; Thirumalai, D.; Garcia-Sakai, V.; Woodson, S.; Sokolov, A. *J. Am. Chem. Soc.* **2006**, *128*, 32.
(4) Doster, W. *Eur. Biophys. J.* **2008**, *37*, 591.
(5) Frauenfelder, H.; Chen, G.; Berendzen, J.; Fenimore, P. W.; Jansson, H.; McMahon, B. H.; Stroe, I. R.; Swenson, J.; Young, R. D. *Proc. Natl. Acad. Sci.* **2009**, *106*, 5129.
(6) Doster, W. *Biochim. Biophys. Acta* **2010**, *1804*, 3.
(7) Zanotti, J.-M.; Bellissent-Funel, M.-C.; Chen, S.-H. *Europhys. Lett.* **2005**, *71*, 91.
(8) Khodadadi, S.; Pawlus, S.; Roh, J. H.; Sakai, V. G.; Mamontov, E.; Sokolov, A. P. *J. Chem. Phys.* **2008**, *128*, 195106.
(9) Zanotti, J.-M.; Gibrat, G.; Bellissent-Funel, M.-C. *Phys. Chem. Chem. Phys.* **2008**, *10*, 4865.
(10) Miyazaki, Y.; Matsua, T.; Suga, H. *J. Phys. Chem. B* **2000**, *104*, 8044.
(11) Doster, W.; Busch, S.; Gaspar, A. M.; Appavou, M.-S.; Wutke, J.; Scheer, H. *Phys. Rev. Lett.* **2010**, *104*, 098101.
(12) Chen, S.-H.; Liu, L.; Fratini, E.; Baglioni, P.; Mamontov, E. *Proc. Natl. Acad. Sci.* **2006**, *103*, 9012.
(13) Kumar, P.; Yan, Z.; Xu, L.; Mazza, M. G.; Buldyrev, S. V.; Chen, S.-H.; Sastry, S.; Stanley, H. E. *Phys. Rev. Lett.* **2006**, *97*, 177802.
(14) Pawlus, S.; Khodadadi, S.; Sokolov, A. P. *Phys. Rev. Lett.* **2008**, *100*, 108103.
(15) Ngai, K. L.; Capaccioli, S.; Shinyashiki, N. *J. Phys. Chem. B* **2008**, *112*, 3826.
(16) Khodadadi, S.; Pawlus, S.; Sokolov, A. P. *J. Phys. Chem. B* **2008**, *112*, 14273.
(17) For supercolled liquids close to the glass transition, the slowest relaxation process is called the α process. It roughly corresponds to molecular rotation in molecular liquids and is often non-Arrhenius. Secondary relaxation processes occurring on shorter time scales are broadly assigned to β-relaxation. The notion of a β-process controlling protein rms atomic displacements and emerging in the observation window at T_{tr} has not been entirely settled. Non-Arrhenius relaxation is seen by broad-band dielectric measurements,[20] and an α-process fits well the protein rms displacements.[4]
(18) Wood, K.; Frölich, A.; Paciaroni, A.; Moulin, M.; Härtlein, M.; Zaccai, G.; Tobias, D. J.; Weik, M. *J. Am. Chem. Soc.* **2008**, *130*, 4586.
(19) Chu, X.-Q.; Faraone, A.; Kim, C.; Fratini, E.; Baglioni, P.; Leao, J. B.; Chen, S.-H. *J. Phys. Chem. B* **2009**, *113*, 5001.
(20) Schirò, G.; Cupane, A.; Vitrano, E.; Bruni, F. *J. Phys. Chem. B* **2009**, *113*, 9606.
(21) He, Y.; Ku, P. I.; Knab, J. R.; Chen, J. Y.; Markelz, A. G. *Phys. Rev. Lett.* **2008**, *101*, 178103.
(22) Johnson, M. E.; Malardier-Jugroot, C.; Murarka, R. K.; Head-Gordon, T. *J. Phys. Chem. B* **2009**, *113*, 4082.
(23) Paciaroni, A.; Cinelli, S.; Onori, G. *Biophys. J.* **2002**, *83*, 1157.
(24) Backus, E. H. G.; Bloem, R.; Pfister, R.; Moretto, A.; Crisma, M.; Toniolo, C.; Hamm, P. *J. Phys. Chem. B* **2009**, *113*, 13405.
(25) LeBard, D. N.; Matyushov, D. V. *Phys. Rev. E* **2008**, *78*, 061901.
(26) Pal, S. K.; Zewail, A. H. *Chem. Rev.* **2004**, *104*, 2099.
(27) Ebbinghaus, S.; Kim, S. J.; Heyden, M.; Yu, X.; Heugen, U.; Gruebele, M.; Leitner, D. M.; Havenith, M. *Proc. Natl. Acad. Sci.* **2007**, *104*, 20749.
(28) Matyushov, D. V. *Phys. Rev. E* **2010**, *81*, 021914.
(29) Nilsson, L.; Halle, B. *Proc. Natl. Acad. Sci.* **2005**, *102*, 13867.
(30) Zhang, L.; Wang, L.; Kao, Y.-T.; Qiu, W.; Yang, Y.; Okobiah, O.; Zhong, D. *Proc. Natl. Acad. Sci.* **2007**, *104*, 18461.
(31) Li, T.; Hassanali, A. A.; Singer, S. J. *J. Phys. Chem. B* **2008**, *112*, 16121.
(32) Sen, S.; Andreatta, D.; Ponomarev, S. Y.; Beveridge, D. L.; Berg, M. A. *J. Am. Chem. Soc.* **2009**, *131*, 1724.
(33) Jimenez, R.; Fleming, G. R.; Kumar, P. V.; Maroncelli, M. *Nature* **1994**, *369*, 471.
(34) Nandi, N.; Bhattacharyya, K.; Bagchi, B. *Chem. Rev.* **2000**, *100*, 2013.
(35) Golosov, A. A.; Karplus, M. *J. Phys. Chem. B* **2007**, *111*, 1482.
(36) Halle, B.; Nilsson, L. *J. Phys. Chem. B* **2009**, *113*, 8210.
(37) Zhou, R.; Huang, X.; Margulis, C. J.; Berne, B. J. *Proc. Natl. Acad. Sci.* **2004**, *305*, 1605.
(38) Berne, B. J.; Weeks, J. D.; Zhou, R. *Annu. Rev. Phys. Chem.* **2009**, *60*, 85.
(39) Makarov, V. A.; Andrews, B. K.; Pettitt, B. M. *Biopolymers* **1998**, *45*, 469.
(40) Giovambattista, N.; Lopez, C. F.; Rossky, P. J.; Debenedetti, P. G. *Proc. Natl. Acad. Sci.* **2008**, *105*, 2274.
(41) ten Wolde, P. R.; Chandler, D. *Proc. Natl. Acad. Sci.* **2002**, *99*, 6539.
(42) Choudhury, N.; Pettitt, B. *J. Am. Chem. Soc.* **2007**, *129*, 4847.
(43) Mittal, J.; Hummer, G. *Proc. Natl. Acad. Sci.* **2008**, *105*, 20130.
(44) Willard, A. P.; Chandler, D. *Faraday Trans.* **2009**, *141*, 209.
(45) Sarupria, S.; Garde, S. *Phys. Rev. Lett.* **2009**, *103*, 037803.
(46) Dadarlat, V. M.; Post, C. B. *Proc. Natl. Acad. Sci.* **2003**, *100*, 14778.
(47) Dadarlat, V. M.; Post, C. B. *Biophys. J.* **2006**, *91*, 4544.
(48) Tarek, M.; Tobias, D. J. *Phys. Rev. Lett.* **2002**, *88*, 138101.
(49) Tournier, A. L.; Xu, J.; Smith, J. C. *Biophys. J.* **2003**, *85*, 1871.
(50) Tarek, M.; Tobias, D. J. *Eur. Biophys J.* **2008**, *37*, 701.
(51) Bergner, A.; Heugen, U.; Bründermann, E.; Schwaab, G.; Havenith, M.; Chamberlin, D. R.; Haller, E. E. *Rev. Sci. Instrum.* **2005**, *76*, 063110.
(52) Knab, J. R.; Chen, J.-Y.; He, Y.; Markelz, A. G. *Proc. IEEE* **2007**, *95*, 1605.
(53) Oleinikova, A.; Sasisanker, P.; Weingärtner, H. *J. Phys. Chem. B* **2004**, *108*, 8467.
(54) Mijović, J.; Bian, Y.; Gross, R. A.; Chen, B. *Macromolecules* **2005**, *38*, 10812.
(55) Ebbinghaus, S.; Kim, S. J.; Heyden, M.; Yu, X.; Gruebele, M.; Leitner, D. M.; Havenith, M. *J. Am. Chem. Soc.* **2008**, *130*, 2374.
(56) Higo, J.; Sasai, M.; Shirai, H.; Nakamura, H.; Kugimiya, T. *Proc. Natl. Acad. Sci.* **2001**, *98*, 5961.
(57) Kuharski, R. A.; Bader, J. S.; Chandler, D.; Sprik, M.; Klein, M. L.; Impey, R. W. *J. Chem. Phys.* **1988**, *89*, 3248.
(58) Blumberger, J.; Sprik, M. *Theor. Chem. Acc.* **2006**, *115*, 113.
(59) Matyushov, D. V. *Acc. Chem. Res.* **2007**, *40*, 294.
(60) Landau, L. D.; Lifshitz, E. M. *Electrodynamics of continuous media*; Pergamon: Oxford, 1984.
(61) Palmer, R. G. *Adv. Phys.* **1982**, *31*, 669.
(62) Marcus, R. A. *J. Phys. Chem.* **1989**, *93*, 3078.
(63) Small, D. W.; Matyushov, D. V.; Voth, G. A. *J. Am. Chem. Soc.* **2003**, *125*, 7470.
(64) LeBard, D. N.; Matyushov, D. V. *J. Chem. Phys.* **2008**, *128*, 155106.
(65) Hansen, J. P.; McDonald, I. R. *Theory of Simple Liquids*; Academic Press: Amsterdam, 2003.
(66) LeBard, D. N.; Matyushov, D. V. *J. Phys. Chem. B* **2008**, *112*, 5218.
(67) LeBard, D. N.; Kapko, V.; Matyushov, D. V. *J. Phys. Chem. B* **2008**, *112*, 10322.
(68) Tan, M.-L.; Dolan, E.; Ichiye, T. *J. Phys. Chem. B* **2004**, *108*, 20435.
(69) Marcus, R. A.; Sutin, N. *Biochim. Biophys. Acta* **1985**, *811*, 265.
(70) Luzar, A.; Chandler, D. *Phys. Rev. Lett.* **1996**, *76*, 928.
(71) Laage, D.; Hynes, J. T. *Science* **2006**, *311*, 832.
(72) Shenogina, N.; Keblinski, P.; Garde, S. *J. Chem. Phys.* **2008**, *129*, 155105.
(73) Lee, C. Y.; McCammon, J. A.; Rossky, P. J. *J. Chem. Phys.* **1984**, *80*, 4448.
(74) Köfinger, J.; Hummer, G.; Dellago, C. *Proc. Natl. Acad. Sci.* **2008**, *105*, 13218.
(75) Mikami, F.; Matsuda, K.; Kataura, H.; Maniwa, Y. *ACS Nano* **2009**, *3*, 1279.
(76) Fedichev, P. O.; Menshikov, L. I. Cornell University Library arXiv database. http://arxiv.org/abs/cond-mat/0601129.
(77) Mazza, M. G.; Stokely, K.; Pagnotta, S. E.; Bruni, F.; Stanley, H. E.; Franzese, G. Cornell University Library arXiv database. http://arxiv.org/abs/0907.1810.
(78) Blinc, R.; Zeks, B. *Soft modes in ferroelectrics and antiferroelectrics*; North-Holland Publishing Co.: Amsterdam, 1974.
(79) Chandler, D. *Nature* **2005**, *437*, 640.
(80) Patel, A. J.; Varilly, P.; Chandler, D. *J. Phys. Chem. B* **2010**, *114*, 1632.
(81) Rodgers, J. M.; Weeks, J. D. *Proc. Natl. Acad. Sci.* **2008**, *105*, 19136.
(82) Henderson, J. R.; Lekner, J. *Mol. Phys.* **1978**, *36*, 781.
(83) Makarov, V. A.; Andrews, B. K.; Smith, P. E.; Pettitt, B. M. *Biophys. J.* **2000**, *79*, 2966.
(84) Halle, B. *Philos. Trans. R. Soc. London* **2004**, *359*, 1207.
(85) Kinoshita, M.; Suzuki, M. *J. Chem. Phys.* **2009**, *130*, 014707.

(86) Qvist, J.; Persson, E.; Mattea, C.; Halle, B. *Faraday Trans.* **2009**, *141*, 131.
(87) Swenson, J.; Teixeira, J. *J. Chem. Phys.* **2010**, *132*, 014508.
(88) Roberts, J. E.; Schnitker, J. *J. Phys. Chem.* **1995**, *99*, 1322.
(89) Rajamani, S.; Truskett, T. M.; Garde, S. *Proc. Natl. Acad. Sci.* **2005**, *102*, 9475.
(90) Landau, L. D.; Lifshits, E. M. *Statistical Physics*; Elsevier: New York, 1980; pp 44 and 260.
(91) Debenedetti, P. G. *Metastable Liquids: Concepts and Principles*; Princeton University Press: Princeton, NJ, 1996.
(92) Elber, R.; Karplus, M. *Phys. Rev. Lett.* **1986**, *56*, 394.
(93) Hunt, N. T.; Kattner, L.; Shanks, R. P.; Wynne, K. *J. Am. Chem. Soc.* **2007**, *129*, 3168.
(94) Rudas, T.; Schröder, C.; Boresch, S.; Steinhauser, O. *J. Chem. Phys.* **2006**, *124*, 234908.
(95) Allen, M. P.; Tildesley, D. J. *Computer Simulation of Liquids*; Clarendon Press: Oxford, 1996.
(96) Wei, D.; Patey, G. N. *Phys. Rev. Lett.* **1992**, *68*, 2043.
(97) Wei, D.; Patey, G. N.; Perera, A. *Phys. Rev. E* **1993**, *47*, 506.
(98) Weis, J.-J. *J. Chem. Phys.* **2005**, *123*, 044503.
(99) Matyushov, D. V. *J. Phys. Chem. B* **2006**, *110*, 10095.
(100) Sharma, M.; Resta, R.; Car, R. *Phys. Rev. Lett.* **2007**, *98*, 247401.
(101) LeBard, D. N.; Matyushov, D. V. *J. Phys. Chem. B* **2009**, *113*, 12424.
(102) Paulo, P. M. R.; Lopes, J. N. C.; Costa, S. M. B. *J. Phys. Chem. B* **2008**, 14779.
(103) Zaccai, G. *Science* **2000**, *288*, 1604.
(104) Ghorai, P. K.; Matyushov, D. V. *J. Phys. Chem. A* **2006**, *110*, 8857.
(105) Martin, D. R.; Matyushov, D. V. *Phys. Rev. E* **2008**, *78*, 041206.
(106) Smith, P. E.; Brunne, R. M.; Mark, A. E.; van Gunsteren, W. F. *J. Phys. Chem.* **1993**, *97*, 2009.
(107) Simonson, T. *Rep. Prog. Phys.* **2003**, *66*, 737.
(108) Simonson, T. *Photosynth. Res.* **2008**, *97*, 21.
(109) Glass, D. G.; Krishnan, M.; Nutt, D. R.; Smith, J. C. *J. Chem. Theory Comput.* **2010**, *6*, 1390.
(110) Kim, S. J.; Born, B.; Havenith, M.; Gruebele, M. *Angew. Chem., Int. Ed.* **2008**, *47*, 6486.
(111) Born, B.; Kim, S. J.; Ebbinghaus, S.; Grueble, M.; Havenith, M. *Faraday Discuss.* **2009**, *141*, 161.
(112) Perticaroli, S.; Comez, L.; Paolantoni, M.; Sassi, P.; Lupi, L.; Fioretto, D.; Paciaroni, A.; Morresi, A. *J. Phys. Chem. B* **2010**, *114*, 8262.
(113) Qin, Z.; Ervin, J.; Larios, E.; Gruebele, M.; Kihara, H. *J. Phys. Chem. B* **2002**, *106*, 13040.
(114) Schmickler, W. *Interfacial Electrochemistry*; Oxford University Press: New York, 1996.
(115) Kümmerle, R.; Gaillard, J.; Kyritsis, P.; Moulis, J.-M. *J. Biol. Inorg. Chem.* **2001**, *6*, 446.
(116) Jasaitis, A.; Rappaport, F.; Pilet, E.; Liebl, U.; Vos, M. H. *Proc. Natl. Acad. Sci.* **2005**, *102*, 10882.
(117) Hirst, J.; Armstrong, F. A. *Anal. Chem.* **1998**, *70*, 5062.
(118) Chi, Q.; Zhang, J.; Andersen, J. E. T.; Ulstrup, J. *J. Phys. Chem. B* **2001**, *105*, 4669.
(119) Jeuken, L. J. C.; McEvoy, J. P.; Armstrong, F. A. *J. Phys. Chem. B* **2002**, *106*, 2304.
(120) Hildebrandt, P.; Murgida, D. H. *Bioelectrochem.* **2002**, *55*, 139.
(121) Guo, Y.; Zhao, J.; Yin, X.; Gao, X.; Tian, Y. *J. Phys. Chem. C* **2008**, *112*, 6013.
(122) Khostariya, D. E.; Dolidze, T. D.; Shushanyan, M.; Davis, K. L.; Waldeck, D. H.; van Eldik, R. *Proc. Natl. Acad. Sci.* **2010**, *107*, 2757.
(123) Monari, S.; Battistuzzi, G.; Borsari, M.; Millo, D.; Gooijer, C.; van der Zwan, G.; Ranieri, A.; Sola, M. *J. Appl. Electrochem.* **2008**, *38*, 885.
(124) Ranieri, A.; Battistuzzi, G.; Borsari, M.; Casalini, S.; Fontanesi, C.; Monari, S.; Siwek, M. J.; Sola, M. *J. Electroanal. Chem.* **2009**, *626*, 123.
(125) Blumberger, J. *Phys. Chem. Chem. Phys.* **2008**, *10*, 5651.
(126) Cascella, M.; Magistrato, A.; Tavernelli, I.; Carloni, P.; Rothlisberger, U. *Proc. Natl. Acad. Sci.* **2006**, *103*, 19641.
(127) Winkler, J. R.; Malmström, B. G.; Gray, H. B. *Biophys. Chem.* **1995**, *54*, 199.
(128) Jasaitis, A.; Johansson, M. P.; Wikström, M.; Vos, M. H.; Verkhovsky, M. I. *Proc. Natl. Acad. Sci.* **2007**, *104*, 20811.
(129) Takayama, S. J.; Irie, K.; Tai, H.; Kawahara, T.; Hirota, S.; Takabe, T.; Alcaraz, L. A.; Donaire, A.; Yamamoto, Y. *J. Biol. Inorg. Chem.* **2009**, *14*, 821.

JP1006999